

## RESEARCH ARTICLE

10.1002/2015JA022163

## Key Points:

- We present new observations of  $F$  region plasma current signatures
- We model the  $F$  region magnetic signatures with line current model
- We compute the self-correlation length of the  $F$  region currents

## Correspondence to:

P. Alken,  
patrick.alken@colorado.edu

## Citation:

Alken, P. (2016), Observations and modeling of the ionospheric gravity and diamagnetic current systems from CHAMP and Swarm measurements, *J. Geophys. Res. Space Physics*, 121, 589–601, doi:10.1002/2015JA022163.

Received 12 NOV 2015

Accepted 15 DEC 2015

Accepted article online 17 DEC 2015

Published online 11 JAN 2016

## Observations and modeling of the ionospheric gravity and diamagnetic current systems from CHAMP and Swarm measurements

P. Alken<sup>1,2</sup><sup>1</sup>University of Colorado Boulder, Boulder, Colorado, USA, <sup>2</sup>National Centers for Environmental Information, Colorado, USA

**Abstract** The CHAMP and Swarm satellites, which provide high-quality magnetic field measurements in low-altitude polar orbits, are ideally suited for investigating ionospheric current systems. In this study, we focus on the  $F$  region low-latitude gravity and diamagnetic currents which are prominent in the equatorial ionization anomaly (EIA) region in the North and South Hemisphere. During its 10 year mission, CHAMP has sampled nearly the entire altitude range of the EIA, offering the opportunity to study these currents from above, inside, and below their source region. The Swarm constellation offers the unique opportunity to study near-simultaneous measurements of the current systems at different longitudinal separations. In this study, we present new observations of these current systems, investigate their seasonal and local time dependence, investigate the use of in situ electron density measurements as a proxy for the magnetic perturbations, and compute the longitudinal self correlation of these currents. We find that these currents are strongest during spring and fall, produce nighttime magnetic fields at satellite altitude of up to 5–7 nT during solar maximum, 2–3 nT during solar minimum, and are highly correlated with in situ electron density measurements. We also find these currents are self-correlated above 70% up to 15° longitude in both hemispheres during the evening.

### 1. Introduction

In the  $F$  region ionosphere at low latitudes, from approximately 150 to 800 km altitude, electrical currents are driven by neutral winds as well as plasma effects. The neutral wind field, blowing across the geomagnetic field induces an electric field which in turn drives a current. This current is in general divergent, and so an additional polarization electric field builds up and continually adjusts itself to ensure the total current is divergence free [Rishbeth, 1971, 1997]. There are additional current systems in the  $F$  region, driven by ionized plasma throughout the ionosphere. In the low-latitude  $F$  region, these currents are significantly enhanced due to regions of increased plasma density on both sides of the magnetic equator, known as the equatorial ionization anomaly (EIA) (see reviews by Anderson [1981] and Stening [1992]). The two distinct current systems driven by plasma density are the gravitational and diamagnetic currents. The gravity current arises from the coupling between the Earth's gravitational and magnetic fields and the charged plasma in the ionosphere. Much like an electric field causes electrons and ions to drift in a magnetic field, the gravitational field also causes motion of the charged particles. The main difference is that an  $F$  region electric field causes ions and electrons to drift in the same direction, while the gravity field causes them to drift in opposite directions, leading to a net current. This current is given by

$$\mathbf{J}_g = \frac{n m_i}{B^2} \mathbf{g} \times \mathbf{B}, \quad (1)$$

where  $n$  is the plasma density,  $m_i$  is the ion mass which carries the current (primarily  $O^+$  in the  $F$  region ionosphere),  $\mathbf{g}$  is the gravity field, and  $\mathbf{B}$  is the geomagnetic field. Due to the dependence on density, we expect this current to be strongest in the ionospheric EIA region in the  $F$  layer. In this low-latitude region, the magnetic field is approximately pointing northward; the gravitational field is vertically down, and so the resulting current will flow in the magnetic eastward direction.

The diamagnetic current can be understood by considering the effect of forces on a plasma due to gradients in the plasma pressure. The diffusion force, which moves plasma from higher to lower pressure regions, will act to drive a current which reduces the magnetic field inside the plasma region. This is why the current is

called diamagnetic. The diamagnetic current is proportional to  $\mathbf{B} \times \nabla P$ , where  $P$  is the plasma pressure. In the ionosphere, we would expect the plasma pressure to have its largest gradients in the boundary region of the EIA, where the density is changing rapidly. At low latitudes, this will drive currents whose magnetic perturbations oppose the main field direction, i.e., approximately southward. When searching for the signals of the gravity and diamagnetic currents in satellite data, it is important to note that the diamagnetic signature will always point southward at low latitudes, while the gravity signature will point southward if measured above the current region, and northward if measured below the current region. We will discuss this further in section 3.

The ionospheric gravity and diamagnetic currents have been investigated in previous studies [Lühr *et al.*, 2003; Eccles, 2004; Maus and Lühr, 2006; Alken *et al.*, 2011], using both physics-based models and direct satellite observations. However, there has not yet been a thorough study of the seasonal and local time behavior of these currents. Furthermore, the observational studies [Lühr *et al.*, 2003; Maus and Lühr, 2006] presented data from CHAMP when it was still flying at a relatively high altitude. These current systems have not yet been investigated using the low-altitude CHAMP data toward the end of its mission. The purpose of this paper is to continue the investigation of these two ionospheric current systems using the full 10 year CHAMP database (2000–2010), as well as 2 years of Swarm data (late 2013–2015). In section 2, we will discuss our methodology of processing the satellite measurements to visualize the signals of these two current systems. In section 3 we present our observations of these current signatures in the satellite data and discuss their seasonal and local time dependence. In section 4, we present a method of estimating equivalent currents from the satellite magnetic measurements on a track-by-track basis and then perform a correlation analysis between near-simultaneous measurements from the Swarm constellation at different longitudes. Finally, we make concluding remarks in section 5.

## 2. Data Processing

In this study, we use magnetic field measurements from both the CHAMP [Reigber *et al.*, 2003] and Swarm [Friis-Christensen *et al.*, 2006] satellite missions. CHAMP (Challenging Minisatellite Payload) was launched in July 2000 into a near-polar orbit with an inclination of  $87^\circ$  and a period of about 93 min. Its initial altitude was 454 km, which decayed to about 250 km by the end of its 10 year mission, in September 2010. This altitude range spans most of the EIA plasma density enhancement at low latitudes, which enables the study of the gravity and diamagnetic current systems from both above and below the main sources. Swarm is comprised of three identical satellites, launched in November 2013. A lower pair (A and C) fly side-by-side in circular polar orbits at an altitude of 460 km with inclinations of  $87.4^\circ$ . The third satellite (B) flies at a higher altitude of 530 km with an inclination of  $88^\circ$ . All three Swarm satellites are currently flying above the region containing most of the plasma density enhancement.

To study the low-latitude  $F$  region current systems, we use the vector fluxgate magnetometer instruments from CHAMP and Swarm. First, a main field model is removed from the vector field measurements. For CHAMP, we use the POMME-6 [Maus *et al.*, 2010] main field model to spherical harmonic degree 15. For Swarm, we used a parent model based on the NOAA candidate to the twelfth generation IGRF [Alken *et al.*, 2015], also to degree 15. Next, for all satellites, we subtract the lithospheric field for degrees 16 to 133 using MF7 [Maus *et al.*, 2008] and the large-scale magnetospheric field using the external CHAOS model [Finlay *et al.*, 2015]. The resulting residuals contain primarily magnetic signatures of the ionospheric  $E$  and  $F$  region sources, induced fields in the Earth due to time-varying external sources, unmodeled external fields (discussed in more detail in section 2.1) as well as unmodeled fields due to errors in the various field models. That is,

$$\mathbf{B}_{\text{residual}} = \mathbf{B}_{\text{ionosphere}} + \mathbf{B}_{\text{induced}} + \mathbf{B}_{\text{external}} + \epsilon, \quad (2)$$

where  $\epsilon$  represents the error in the various field models. The residuals could also contain fields due to smaller sources, such as ocean-driven currents, which we will consider part of the error term  $\epsilon$ . For each orbit, we then calculate along-track root-mean-square (RMS) values for the residuals in each vector component and discard tracks with large RMS, which could indicate instrument errors, stray spacecraft fields, or other sources of noise.

In addition to the magnetometer data, we investigated in situ measurements of the electron density made by the Langmuir probe instruments on CHAMP and Swarm. While the currents themselves are driven by the plasma distribution throughout the EIA region, the in situ measurements often provide a reliable proxy for

the expected magnetic perturbations. We used the Langmuir probe data from both satellite missions with no additional processing.

### 2.1. Along-Track Differences

Due to the quality of low-Earth orbiting satellite measurements during the CHAMP and Swarm years, internal main and lithospheric field models have been produced which can describe the geomagnetic field at satellite altitude very accurately. When attempting to isolate ionospheric fields in the measurements, the main source of unwanted signal comes from induced and external (magnetospheric) fields, which are much more difficult to model on a track-by-track basis. These fields can vary rapidly in both time and spatial structure due to solar activity, and models of these sources typically rely on indices such as *Dst*, which have known baseline inaccuracies. Therefore, while the procedure described above removes some of these signals, there remains some significant unmodeled signal in the residuals due to these sources. At low latitudes, the horizontal field component is particularly contaminated by unmodeled external fields. In order to remove these unwanted fields, and preserve the ionospheric signals of interest, we investigated the use of along-track differences. Along-track differences have recently been reported to be very useful in removing external fields and recovering clean lithospheric signals in satellite data [Kotsiaros *et al.*, 2015]. The idea is to take a vector measurement at some time  $t$  and position  $\mathbf{r}_1$ , and a second measurement a short time later along the track, corresponding to time  $t + \delta t$  and position  $\mathbf{r}_2$  and subtract them. According to equation (2), this will yield

$$\delta \mathbf{B}_{\text{residual}} = \delta \mathbf{B}_{\text{ionosphere}} + \delta \mathbf{B}_{\text{induced}} + \delta \mathbf{B}_{\text{external}} + \delta \epsilon, \quad (3)$$

where  $\delta \mathbf{B}_{\text{residual}} = \alpha (\mathbf{B}_{\text{residual}}(t + \delta t, \mathbf{r}_2) - \mathbf{B}_{\text{residual}}(t, \mathbf{r}_1))$  and similarly for the other terms in equation (3). The coefficient  $\alpha$  is taken to be +1 for north-flying tracks and  $-1$  for south-flying tracks. This ensures the same sign of the residual regardless of the satellite flight direction. Since the unwanted induced and external current sources are far away from the satellites compared to the ionospheric sources of interest, their fields have larger spatial scales (or lower frequencies when viewed as along-track time series), and so by an appropriate choice of  $\delta t$ , we can significantly remove these large-scale fields, while preserving the smaller-scale ionospheric signals. In some sense, along-track differencing acts as a high-pass filter, removing low-frequency fields due to sources further away, while preserving high-frequency fields due to sources closer to the satellite. After some experimentation, we selected the time interval  $\delta t = 40$  sec, which corresponds to the satellite moving by approximately  $1.5^\circ$  in latitude. This value appeared to offer a good trade-off between preserving the *F* region signatures and removing the large-scale external and induced fields, which do not vary too much over small latitude ranges.

## 3. Observations

In the low-latitude EIA region, the magnetic field lines are approximately pointing northward, and so the gravity-driven  $\mathbf{g} \times \mathbf{B}$  current will flow in the magnetic eastward direction. The magnetic signature of this current is therefore expected to be most prominent in the  $B_x$  (north) and  $B_z$  (vertical) field components. Above the current system, the  $B_x$  component will point southward, with its strongest magnitude occurring near the peak density region. Below the current system, the  $B_x$  component will change sign and point northward. The  $B_z$  component is mostly independent of altitude, pointing radially downward in the Southern Hemisphere, radially upward in the Northern Hemisphere, and changes sign near the magnetic equator.

The diamagnetic current signature opposes the ambient field and so appears in the opposite of the total field (*F*) direction. Above the current region, the signature of this current will look very similar to the gravity signature in both the  $B_x$  and  $B_z$  components. However, below the current region, the  $B_x$  component will continue to point southward, while the gravity  $B_x$  points northward. This feature offers us an opportunity to visually separate these two current systems in the low-altitude CHAMP measurements.

### 3.1. Satellite Track Analyses

Figure 1 shows single-track measurements of these *F* region currents at two different altitudes during the evening when the *E* region *Sq* and equatorial electrojet (EEJ) current systems are not present. The left column shows a track from Swarm B near 500 km altitude and 1958 local time on 5 February 2014. At this altitude, we expect most of the enhanced plasma density (and corresponding currents) to be below the satellite. The top panel shows the  $B_x$  residual which exhibits a southward field near  $+10.5$  and  $-15.5^\circ$  quasi-dipole latitude, indicated by the vertical lines. This is consistent with the field of a magnetic eastward current flowing below

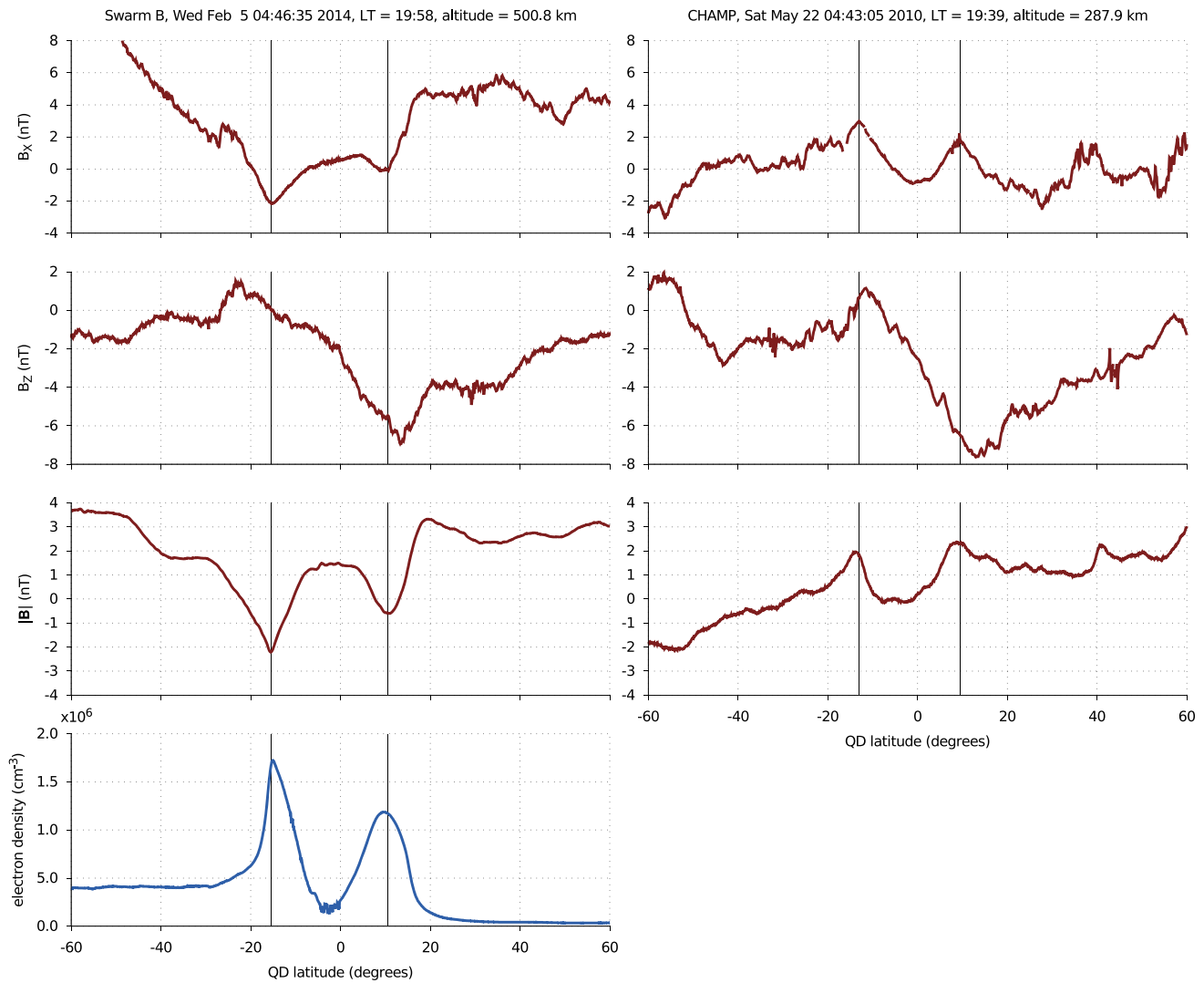


**Figure 1.** (left column)  $B_x$ ,  $B_z$ , and total field magnetic residuals, including in situ electron density measurements for a single track from Swarm B on 5 February 2014. Vertical lines are drawn at  $-15.5^\circ$  and  $10.5^\circ$  quasi-dipole (QD) latitude. (right column)  $B_x$ ,  $B_z$ , and total field magnetic residuals for a single track from CHAMP on 22 May 2010. Electron density measurements were not available for CHAMP on this day. Vertical lines are drawn at  $-13^\circ$  and  $9.5^\circ$  QD latitude. Both satellites were in local times between 1930 and 2000.

the satellite and in the EIA region. The second panel shows the  $B_z$  residual which changes sign across the magnetic equator as expected. The third panel shows the scalar field residuals whose two peaks are well aligned with the  $B_x$  component. The fourth panel shows the in situ electron density measurements from the Langmuir probe instrument which clearly exhibit the two enhanced plasma density regions on both sides of the magnetic equator. The in situ electron density peaks are remarkably well aligned with the features seen in the  $B_x$  and total field residuals. While the fields due to the gravity and diamagnetic currents depend also on plasma density far from the satellite, the along-track in situ measurements often provide a good proxy. For example, the density in the Southern Hemisphere shows a sharper peak than in the Northern Hemisphere, which is reproduced well in the total field residuals.

Figure 1 (right column) shows data for a single CHAMP track near the end of its mission on 22 May 2010 with an altitude of 287.9 km and near 1939 local time. At this low altitude, the bulk of the EIA density enhancement is above the satellite. There is no available Langmuir probe data from CHAMP after February 2010, and so we plot only the  $B_x$ ,  $B_z$  and total field residuals. We find very similar structure in the  $B_z$  component compared with the higher altitude Swarm B data; however, the two low-latitude peaks in the  $B_x$  and total field data are positive, indicating a northward instead of southward field. The sign change of  $B_x$ , coupled with the similarity in  $B_z$

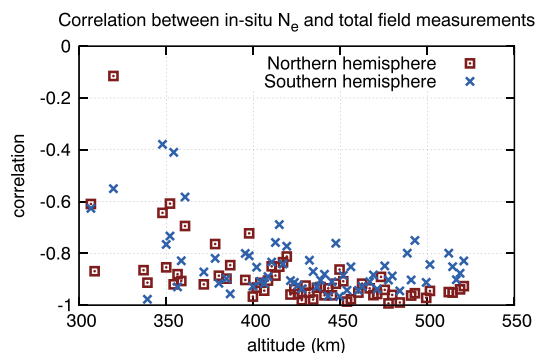


**Figure 2.** Correlation between in situ electron density peaks and corresponding total field perturbations for Northern (red) and Southern (blue) Hemispheres, plotted as a function of satellite altitude. All CHAMP and Swarm data were selected for spring and fall seasons and between 1600 and 2300 local time.

at the two different altitudes rules out the possibility that these signals are due to external magnetospheric fields or fields coming from the  $E$  region ionosphere or induced fields in the Earth. The currents producing these fields are originating inside the EIA enhancement in the  $F$  region of the ionosphere.

While these signals include contributions from both gravity and diamagnetic currents, we can be sure there is a strong gravity contribution as we would not expect a sign change in  $B_x$  from diamagnetic currents, which always produce fields opposing the ambient geomagnetic field. At high altitudes, above the EIA region, the gravity and diamagnetic fields will add to produce a southward  $B_x$ . At low altitudes, below the EIA region, the diamagnetic field will continue to point southward, but the gravity field will change sign and produce a northward  $B_x$ . For this particular CHAMP orbit, the gravity signal has a larger magnitude than the diamagnetic signal in order to produce the observed sign change in  $B_x$ .

In order to further investigate the relationship between the in situ electron density and corresponding total field perturbation, we performed a track-by-track correlation analysis on the two signals. First, we identified peaks in the  $N_e$  measurements by searching for zero crossings of the along-track first derivative. When a peak was found, we searched for a corresponding extremum in the total field residual within  $\pm 5^\circ$  QD latitude of the  $N_e$  peak. This was done due to the observation that the peak in the  $N_e$  signal could often be shifted by a few degrees in latitude from the corresponding peak in the magnetic field measurement. Then we computed the correlation coefficient between the two signals centered on the identified peaks and extending  $\pm 10^\circ$  QD latitude from the peak. This latitude range was found to be adequate to capture the structure of both the  $N_e$  and  $F$  signals. The Northern and Southern Hemispheres were treated separately, and we used tracks only during spring and fall seasons and between 1600 and 2300 local time. All track-by-track correlations for CHAMP and Swarm were combined and binned in altitude. The results are shown in Figure 2. We find for the Northern Hemisphere peak a very high anticorrelation of less than  $-0.80$  between  $N_e$  and  $F$  at high altitudes. Below about 400 km altitude, the correlation grows weaker since the satellite is flying inside the current region, and currents above and below the satellite can reduce the magnetic perturbation. At lower altitudes, we would expect the correlation to go positive, due to the sign change in the  $B_x$  and total field residuals as seen in Figure 1 (right column). However, it is not currently possible to investigate this due to the lack of CHAMP Langmuir probe data after February 2010. The correlation of  $N_e$  and  $F$  in the Southern Hemisphere has a very similar altitude dependence as the Northern Hemisphere, with a larger scatter at high altitudes. This could be due to the generally reduced plasma density in the Southern Hemisphere relative to the Northern Hemisphere. However, we still find a strong anticorrelation between  $N_e$  and  $F$  at high altitudes, with a reduced correlation at lower altitudes in the  $F$  region.

### 3.2. Seasonal Structure

In Figure 3 we plot the CHAMP in situ electron density measurements (a and c) and the vertical field residuals after removing the internal and external field models as discussed in section 2 (b and d). The data are selected for nighttime (19–22 LT) in order to eliminate signatures of  $E$  region current systems like  $Sq$  and EEJ and then binned in QD latitude and season with  $5^\circ$  by 20 day bin sizes. The CHAMP data set is also divided into two approximate 5 year periods, covering July 2000 to December 2005 and January 2006 to September 2010. This is done for two reasons. First, 5 years is about the time period needed for CHAMP to provide even local

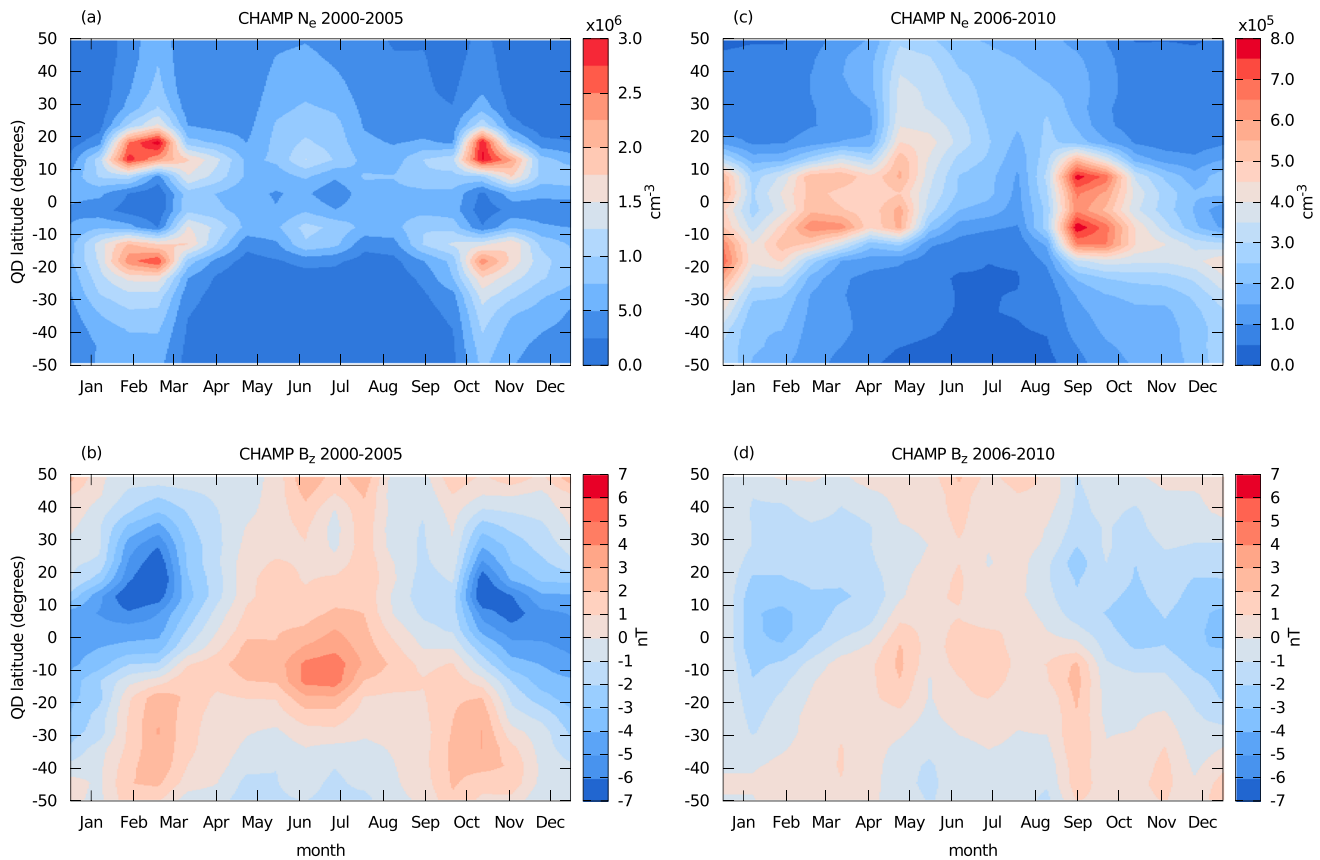


**Figure 3.** (a, c) Seasonal structure of CHAMP electron density measurements for solar maximum years (a) and solar minimum years (c). Note the different scales. (b, d) Seasonal structure of CHAMP vertical field component after removing internal and external field models for solar maximum years (b) and solar minimum years (d). All data were selected for 19–22 local time.

time coverage at all seasons [Lühr *et al.*, 2014]. Second, the first 5 year interval corresponds well with solar maximum (average solar flux index  $F_{10.7} = 141 \pm 46$  sfu), while the second interval corresponds well with solar minimum (average  $F_{10.7} = 74 \pm 7$  sfu).

It is instructive to examine the vertical field component for several reasons. First, at low latitudes, large-scale magnetospheric fields primarily affect the horizontal component, with minimal influence on the vertical component. Second, for the *F* region gravity and diamagnetic currents, the vertical component has a similar structure regardless of CHAMP's altitude, which changed by 200 km during the 10 year mission. The  $B_x$  component is highly sensitive to how much current is flowing above and below the satellite, and since CHAMP is flying in the EIA region throughout its mission, it is difficult to visualize the  $B_x$  structure at all local times and seasons, since CHAMP is continually dropping in altitude. The left column of the figure shows the solar maximum period. In the electron density map (Figure 3a), we see the two EIA peaks about 15° off the magnetic equator for the spring and fall seasons and much reduced density during summer/winter. We also note the asymmetry between the peaks, with more plasma density present in the Northern Hemisphere for both spring and fall. Since the plasma currents are proportional to the density, we would expect the current strength to follow the same pattern. In Figure 3b, we see a sign change in the vertical component as CHAMP crosses the magnetic equator during spring and fall, in very good agreement with the density measurements. For both spring and fall, the zero crossing of  $B_z$  actually occurs about 10° south of the magnetic equator. This is caused by the north/south asymmetry in the electron density. Stronger plasma currents flow in the Northern Hemisphere due to the larger density causing  $B_z$  to change sign in the Southern Hemisphere. During summer and winter, we see a much different signature in  $B_z$ . In May through August, we see a positive  $B_z$  near the magnetic equator, while in December and January  $B_z$  goes negative in this region. From the much

weaker plasma density measurements during these months, we would expect reduced plasma currents, and so these signatures are likely due to other ionospheric current systems flowing during these seasons, such as interhemispheric field-aligned currents.

Figures 3c and 3d show the same measurements for the solar minimum years. From the electron density measurements (Figure 3c), we see again peaks during spring and fall; however, the peaks have shifted slightly. Note the different scale size from the solar maximum plot in order to visualize the much reduced plasma density. In spring during solar maximum, the peak density occurred during February/March, while in solar minimum the density is present from February to May. Also, in fall the peaks shift from October/November during solar maximum to September/October during solar minimum. Additionally, we see the EIA peaks closer to the magnetic equator during solar minimum, most likely due to the smaller vertical range of the plasma fountain during reduced solar activity periods. We again expect the behavior of the plasma currents to follow the density structure. Figure 3d shows the corresponding  $B_z$  measurements for these years. We again find a sign change in the  $B_z$  component across the magnetic equator, which is well aligned with the seasonal structure of the plasma density. We find similar positive/negative features in  $B_z$  during summer/winter as during solar maximum. The strength of the nighttime  $B_z$  signature of the gravity current at CHAMP altitude is about 2–3 nT during solar minimum, compared with 5–7 nT during solar maximum.

It would be very instructive to examine the seasonal dependence of the  $B_x$  component during nighttime as well, but as discussed previously, this component is highly sensitive to the amount of plasma current flowing above and below the observation point, and CHAMP provides measurements only within the plasma enhancement region with steadily decreasing altitude. Swarm, which is currently flying above most of the EIA region, offers a good possibility of analyzing the  $B_x$  component, but since it is less than 2 years into the mission, Swarm has not yet sampled all seasons at all local times. In a few more years, it will be possible to perform a more comprehensive analysis of the high-altitude  $B_x$  signature of the plasma currents.

### 3.3. Local Time Structure

As discussed in section 3.2, we find the strongest signature of the  $F$  region plasma currents during spring and fall. In order to investigate the local time structure of these currents, we selected CHAMP data for spring (February to May) and fall (September to November) and binned the  $B_z$  residuals in QD latitude and local time, with  $5^\circ$  by 1 h bin sizes. The CHAMP data set is again separated into two 5 year periods as before. The results are shown in Figure 4. Due to the strong signature of the  $E$  region  $Sq$  and EEJ currents in the vertical component, we show only data after 19 LT. We again see the characteristic sign change in the  $B_z$  component north and south of the magnetic equator, indicative of an  $F$  region gravity or diamagnetic current. During the solar maximum period (top), the signal lasts until about 22 LT, while during solar minimum (bottom), we see the signal until midnight. This could be due to strong  $F$  region dynamo currents flowing late at night during the solar maximum years and masking the plasma currents, which may have a lesser effect at solar minimum. The solar minimum plot has important implications for main field modeling, as many modelers select quiet-time data starting after 22 LT, assuming that during this period ionospheric currents are negligible [Thébault *et al.*, 2015, and references therein].

To visualize the signatures of the gravity and diamagnetic currents at all local times, we may use along-track differences, as discussed in section 2.1, which act as a high-pass filter and remove much of the large-scale fields due to  $Sq$ , magnetospheric and induced sources. Figure 5 shows the local time structure of the  $B_x$  component plotted as along-track differences from the combined CHAMP and Swarm data sets during the spring and fall seasons. Since the  $B_x$  component is highly sensitive to altitude as discussed previously, we use only data above 430 km altitude. Below  $10^\circ$  QD latitude, we see a very strong feature from 6 to 18 local time which changes sign across the magnetic equator. This is the equatorial electrojet signature, which has a negative slope in the Southern Hemisphere and positive slope in the Northern Hemisphere, as seen by a satellite flying above the  $E$  region. From 6 to 8 local time, we can see a sign change in this low-latitude feature, indicating a counter electrojet. The magnitude of the EEJ signature in terms of along-track differences spaced  $1.5^\circ$  apart in latitude is about 5 nT. From the figure we can also see features on the order of 1–2 nT at about  $\pm 20^\circ$  QD latitude. Due to the differences in magnitude of these features compared to the EEJ, we use a nonlinear color scale which is roughly linear in the range  $-1$  to  $+1$  nT in order to bring out the weaker signatures and then rapidly increases to 5 nT to capture the EEJ variations. We see that the weaker signals at  $\pm 20^\circ$  begin at around 8–9 LT but continue well past 22 LT. This is consistent with the local time dependence of the EIA. Furthermore, the features are highly localized in the latitude region of the EIA. While the signal after 18 LT is almost certainly due to  $F$  region

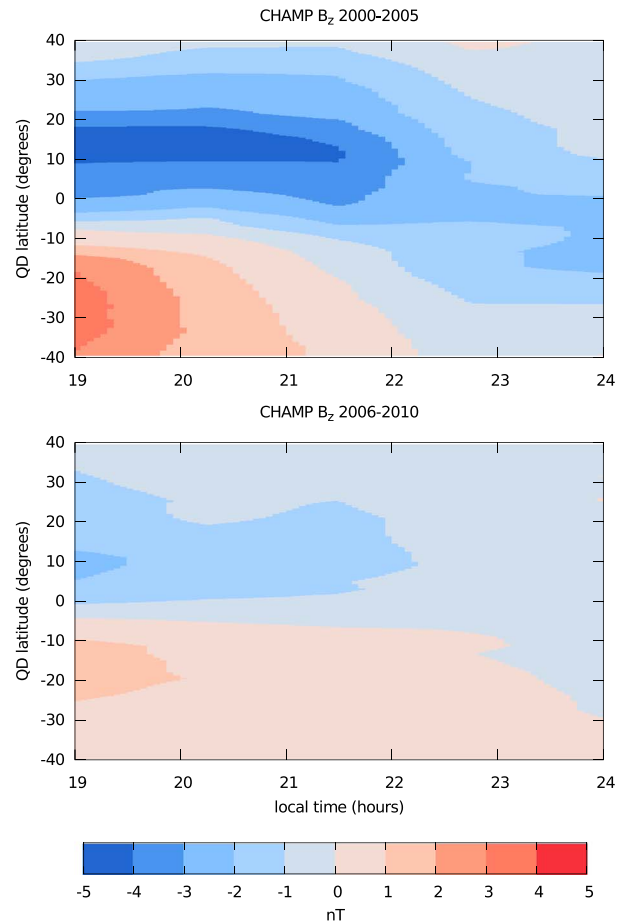


**Figure 4.** Local time structure of CHAMP nighttime vertical field component for (top) solar maximum years and (bottom) solar minimum years. Data were selected for spring and fall seasons.

plasma currents, we cannot state with complete certainty that the daytime signal is coming from the same currents, since at least part of this signal could be coming from the *E* region *Sq* system. However, since *Sq* is a much larger-scale current system, we believe it is unlikely to exhibit such a localized feature exactly in the EIA region. To be completely sure, it would be instructive to look for a sign change in the daytime  $B_x$  component using the low-altitude CHAMP database, say from the spring or fall of 2010. Efforts are currently underway to

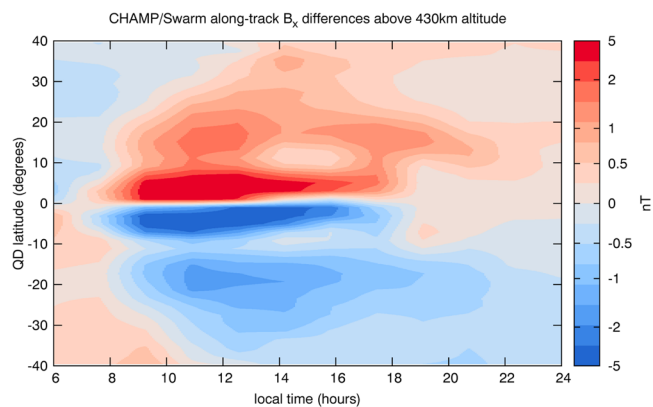


**Figure 5.** Along-track differences in the  $B_x$  component from CHAMP and Swarm data sets, above 430 km altitude, selected for spring and fall, and plotted as a function of local time and QD latitude. A nonlinear color scale is used to visualize the strong EEJ signal below 10° QD latitude as well as the weaker plasma current signatures at  $\pm 20^\circ$  QD latitude.

improve the low-altitude vector CHAMP data to correct issues in the star camera processing (Michaelis, private communication, 2015), and so we will leave this analysis to a future study.

#### 4. Correlation Length of the $F$ Region Plasma Currents

In this section, we investigate the longitudinal correlation length of the  $F$  region plasma current systems. To do this, we will compare near-simultaneous measurements of the currents at different longitudes from the Swarm A and B satellites. At the beginning of the Swarm mission, the A and B satellites were flying very close together, but as the mission progresses, the longitudinal (and local time) separation of the satellites increases. In order to correlate the near-simultaneous current signatures at different longitudes, we first invert the magnetic measurements for line currents flowing in the  $F$  region. The magnetic measurements of  $F$  region currents will vary according to satellite altitude, and since Swarm B flies significantly higher than A, it is necessary to map their magnetic observations onto a current model at a fixed altitude in order to compare them. The inversion procedure we use to determine the line currents was initially developed for equatorial electrojet studies [Lühr *et al.*, 2004] and closely follows that of the Level-2 Swarm equatorial electric field chain [Alken *et al.*, 2013]. There are however a few differences and so we will briefly describe the procedure used here and refer the interested reader to those papers for full technical details.

We define  $N_C = 240$  segmented line currents flowing longitudinally eastward and following lines of constant quasi-dipole latitude. The currents are defined between  $\pm 30^\circ$  quasi-dipole latitude, leading to a spacing of  $0.25^\circ$  between each current. In order to account for the curvature of the Earth, each current is divided into longitudinal segments spanning  $1^\circ$  of longitude with the endpoints of each segment fixed at an altitude of 350 km (roughly the center of the density enhancement region). See Figure 2 of Alken *et al.* [2013] for more details. Each longitudinal segment is treated as a straight line current which contributes linearly to the magnetic field measured at satellite altitude. According to the Biot-Savart law, the unit magnetic field at a position  $\mathbf{r}_i$  due to the linear segment  $k$  of the  $j$ th current arc is

$$d\mathbf{B}_{jk}(\mathbf{r}_i) = \frac{\mu_0}{4\pi} \delta_{jk} \frac{\mathbf{l}_{jk} \times (\mathbf{r}_i - \mathbf{r}_{jk})}{|\mathbf{r}_i - \mathbf{r}_{jk}|^3}, \quad (4)$$

where  $\delta_{jk}$  is the length of segment  $k$  of current  $j$  in meters,  $\mathbf{r}_{jk}$  is a position vector pointing to the midpoint of line segment  $k$  of current  $j$  and  $\mathbf{l}_{jk}$  is a unit vector pointing along the line segment which represents the direction of current flow. In the inversion, all unit vectors  $\mathbf{l}_{jk}$  of the same current arc  $j$  will be multiplied by a scalar  $S_j$ , with units of amperes to yield the final current strength. There are  $N_C$  unknown current strengths  $S_j$ , and the modeled scalar magnetic field at a satellite position  $\mathbf{r}_i$  is given by

$$M(\mathbf{r}_i) = \sum_{j=1}^{N_C} S_j F_j(\mathbf{r}_i), \quad (5)$$

where  $F_j(\mathbf{r}_i)$  is the scalar magnetic field strength at position  $\mathbf{r}_i$  due to current arc  $j$  with a unit current strength, given by

$$F_j(\mathbf{r}_i) = \left( \sum_k d\mathbf{B}_{jk}(\mathbf{r}_i) \right) \cdot \hat{\mathbf{b}}_i, \quad (6)$$

where  $\hat{\mathbf{b}}_i$  is a unit vector in the main field direction at position  $\mathbf{r}_i$ . Here we are simply summing up the field contributions of each longitudinal segment  $k$ , and taking the component along the main field direction. Organizing all satellite scalar measurements along a track into a vector  $\mathbf{y}$ , we can write

$$\mathbf{y} = \mathbf{M}\mathbf{s}, \quad (7)$$

where  $\mathbf{M}$  is a matrix whose elements are given by  $M_{ij} = F_j(\mathbf{r}_i)$  and  $\mathbf{s}$  is a vector of the unknown current strengths  $S_j$ . The current strengths  $S_j$  are then determined by minimizing the linear least squares cost function

$$\chi^2 = \|\mathbf{y} - \mathbf{M}\mathbf{s}\|^2 + \lambda^2 \|\mathbf{L}_2 \mathbf{s}\|^2, \quad (8)$$

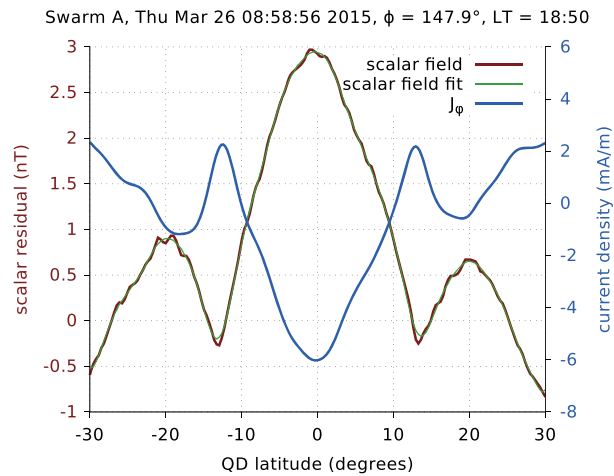


**Figure 6.** Example line current inversion for a single track from Swarm A on 26 March 2015 at 1850 local time. The red curve shows the scalar field residual after removing core, crustal, and external field models. We see a characteristic dip in the scalar residual at  $\pm 12^\circ$  QD latitude due to the *F* region plasma currents. The blue curve shows the derived current density using a line current model at 350 km altitude. Positive current density indicates eastward flow, while negative density indicates westward flow.

where  $\lambda$  is a regularization parameter and  $L_2$  is a second order finite difference operator designed to enforce a smooth solution vector, and given by

$$L_2 = \begin{pmatrix} 1 & -2 & 1 & & \\ & \ddots & \ddots & \ddots & \\ & & 1 & -2 & 1 \end{pmatrix}. \tag{9}$$

For each track, the optimal regularization parameter  $\lambda$  is computed by finding the corner of the corresponding L-curve [Hansen and O’Leary, 1993]. Finally, the height-integrated eastward current density is obtained by dividing the line current strength by the latitudinal distance  $d$  between the line currents,

$$J_\phi(\theta_j) = \frac{S_j}{d}. \tag{10}$$

A spacing of  $0.25^\circ$  QD latitude leads to a distance of approximately  $d \approx 28.3$  km.

We inverted the scalar measurements from Swarm A and B for all tracks between 26 November 2013 to 23 September 2015 and between 1830 and 2300 local time. The analysis was restricted to the evening sector to avoid difficulties in removing the daytime *E* region currents. We further restricted the analysis to only spring and fall seasons, as discussed in section 3.2. This led to a total of 1802 tracks for Swarm A and 1777 tracks for Swarm B. The scalar magnetic measurements for each track were inverted for the equivalent line currents at 350 km altitude, as described above. An example profile from Swarm A on 26 March 2015 is shown in Figure 6. Here the satellite is near 1850 local time and so we would expect no *E* region current signatures. The red curve shows the scalar field residual after removing a core, crustal and external field. We see a depression in the scalar field residual of about 1 nT near  $\pm 12^\circ$  QD latitude, which is characteristic of the *F* region current signatures. The blue curve shows the resulting line current distribution from our inversion. The line current model correctly determines an eastward current flow in the region of these scalar field depressions. The green curve shows the fit of the model to the data. In order to test that the derived current densities are robust to the defined line current geometry, we performed additional inversions with cutoff latitudes larger than  $30^\circ$ , and found that the derived current densities in the EIA region changed very little. Therefore, even though for many tracks there is nonzero magnetic signal at  $30^\circ$  QD latitude (as in Figure 6), this cutoff value is sufficiently far from the EIA region to provide robust current estimates of the gravity and pressure gradient currents.

In order to correlate the *F* region currents in longitude, we searched for equator crossings of Swarm A and B within 30 min of each other. The 30 min was chosen to get a good distribution of near-simultaneous crossing events to make a meaningful correlation. For each crossing event, we compared the peak current values

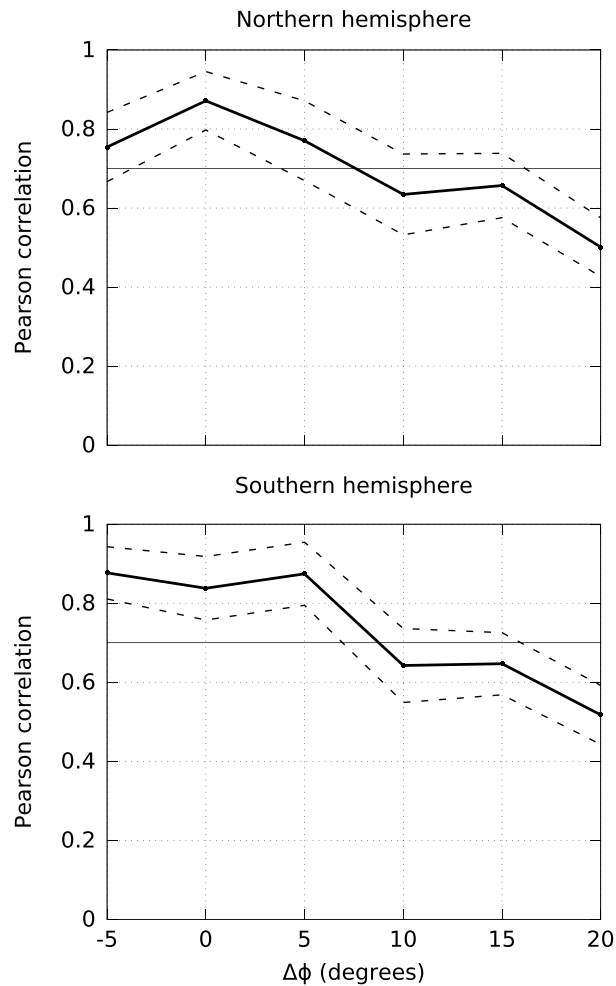


**Figure 7.** Correlation between temporally close measurements of the  $F$  region current density from Swarm A and B plotted as a function of longitudinal distance between the two satellites. The solid line shows the Pearson correlation coefficient, while the dashed lines show the standard error of the correlation coefficient. The horizontal line shows the 70% correlation level. The Northern Hemisphere correlation is shown in the top plot, while the Southern Hemisphere correlation is shown in the bottom.

between the Swarm A and B derived currents, treating the Northern and Southern Hemispheres separately. To locate the peak current value for each profile, we used a simple method which searched for zero crossings of the along-track first derivative of the current. Early in the Swarm mission, the longitude separation between A and B was small, and it continues to grow as the mission progresses. For the time period we considered, the maximal longitudinal separation is about  $25^\circ$ , which is adequate to investigate the longitudinal correlation length of these  $F$  region currents. We binned the near-simultaneous crossing events as a function of the longitudinal separation between A and B, with bin sizes of  $5^\circ$ . We then computed the Pearson correlation of the peak current values of each bin separately for the Northern and Southern Hemispheres. The results are shown in Figure 7.

The longitudinal correlation of the Northern Hemisphere current peaks is shown in the top plot (thick solid) with the standard error shown as dashed. The horizontal 70% correlation threshold is also shown. The bottom plot shows the same quantities for the Southern Hemisphere current peaks. In both hemispheres, the correlation drops below 70% after about  $15^\circ$  longitudinal separation. This is similar to the  $15^\circ$  length found for the equatorial electrojet [Alken and Maus, 2007], even though the  $E$  and  $F$  region current systems are driven by very different mechanisms. For the  $F$  region gravity current, physics-based modeling studies have found that polarization electric fields drive a westward return current through the  $E$  region during the daytime, with the polarization electric field changing from westward to eastward during the late evening [Richmond and Maute, 2014]. This change in the polarization electric field during the evening could be responsible for the reduction

in the longitudinal correlation of these currents during the nighttime. Additional reduction in the plasma density in the late evening would also contribute to smaller correlation lengths. While this study is restricted to analyzing the correlation length during the evening, there is a possibility of finding longer correlation lengths of these currents during daytime, which we plan to investigate in a future study.

## 5. Conclusions

We have presented new observations of the  $F$  region gravity and diamagnetic current systems, using 10 years of CHAMP data and an additional 2 years of Swarm data. The 10 year CHAMP database allows us to observe the signature of these currents from both above and below their primary sources. The main conclusions from this study are as follows.

1. We find a sign change in the  $B_x$  and total field components as CHAMP descends from high to low altitude, indicating the presence of an  $F$  region gravity current which is strong enough to counteract the effects of the diamagnetic current.
2. The total field perturbations of the  $F$  region plasma currents at high altitudes are highly correlated with the in situ Langmuir probe electron density measurements. At altitudes inside the EIA region the correlation decreases due to the reduced magnetic field perturbations of these currents.
3. The  $F$  region gravity and diamagnetic currents are strongest during spring and fall seasons, corresponding well with the seasonal dependence of the EIA.
4. These currents can produce perturbations of one to a few nT in low-Earth orbiting satellite measurements, even up to midnight during both solar maximum and minimum. A better understanding of these signatures could allow improved source separation in main field modeling.
5. The use of along-track differences offers a promising means to visualize these currents in the  $B_x$  component at all local times, although the extent that  $Sq$  contaminates the signal during daytime remains to be investigated.
6. The  $F$  region plasma currents have a self correlation above 70% for longitudinal separations below  $15^\circ$  in both hemispheres.

## Acknowledgments

The operational support of the CHAMP mission by the German Aerospace Center (DLR) is gratefully acknowledged, and CHAMP data can be downloaded from <http://isdc.gfz-potsdam.de>. We acknowledge the support of the Swarm mission from the European Space Agency (ESA). Swarm Level 1b data are available from ESA at <https://earth.esa.int/web/guest/swarm/data-access>.

## References

- Alken, P., and S. Maus (2007), Spatio-temporal characterization of the equatorial electrojet from CHAMP, Ørsted, and SAC-C satellite magnetic measurements, *J. Geophys. Res.*, *112*, A09305, doi:10.1029/2007JA012524.
- Alken, P., S. Maus, A. D. Richmond, and A. Maute (2011), The ionospheric gravity and diamagnetic current systems, *J. Geophys. Res.*, *116*, A12316, doi:10.1029/2011JA017126.
- Alken, P., S. Maus, P. Vigneron, O. Sirol, and G. Hulot (2013), Swarm SCARF equatorial electric field inversion chain, *Earth Planets Space*, *65*(11), 1309–1317, doi:10.5047/eps.2013.09.008.
- Alken, P., S. Maus, A. Chulliat, and C. Manoj (2015), NOAA/NGDC candidate models for the 12th generation International Geomagnetic Reference Field, *Earth Planets Space*, *67*(1), 68, doi:10.1186/s40623-015-0215-1.
- Anderson, D. N. (1981), Modeling the ambient, low latitude F-region ionosphere—A review, *J. Atmos. Terr. Phys.*, *43*(8), 753–762.
- Eccles, J. V. (2004), The effect of gravity and pressure in the electrodynamics of the low-latitude ionosphere, *J. Geophys. Res.*, *109*, A05304, doi:10.1029/2003JA010023.
- Finlay, C., N. Olsen, and L. Tøffner-Clausen (2015), DTU candidate field models for IGRF-12 and the CHAOS-5 geomagnetic field model, *Earth Planets Space*, *67*(1), 114, doi:10.1186/s40623-015-0274-3.
- Friis-Christensen, E., H. Lühr, and G. Hulot (2006), Swarm: A constellation to study the Earth's magnetic field, *Earth Planets Space*, *58*, 351–358.
- Hansen, P. C., and D. P. O'Leary (1993), The use of the L-curve in the regularization of discrete ill-posed problems, *SIAM J. Sci. Comput.*, *14*(6), 1487–1503, doi:10.1137/0914086.
- Kotsiaros, S., C. C. Finlay, and N. Olsen (2015), Use of along-track magnetic field differences in lithospheric field modelling, *Geophys. J. Int.*, *200*(2), 880–889, doi:10.1093/gji/ggu431.
- Lühr, H., M. Rother, S. Maus, W. Mai, and D. Cooke (2003), The diamagnetic effect of the equatorial Appleton anomaly: Its characteristics and impact on geomagnetic field modeling, *Geophys. Res. Lett.*, *30*(17), 1906, doi:10.1029/2003GL017407.
- Lühr, H., S. Maus, and M. Rother (2004), Noon-time equatorial electrojet: Its spatial features as determined by the CHAMP satellite, *J. Geophys. Res.*, *109*, A01306, doi:10.1029/2002JA009656.
- Lühr, H., C. Xiong, J. Park, and J. Rauberg (2014), Systematic study of intermediate-scale structures of equatorial plasma irregularities in the ionosphere based on CHAMP observations, *Frontiers Phys.*, *2*(15), doi:10.3389/fphy.2014.00015.
- Maus, S., and H. Lühr (2006), A gravity-driven electric current in the Earth's ionosphere identified in CHAMP satellite magnetic measurements, *Geophys. Res. Lett.*, *33*, L02812, doi:10.1029/2005GL024436.
- Maus, S., F. Yin, H. Lühr, C. Manoj, M. Rother, J. Rauberg, I. Michaelis, C. Stolle, and R. D. Müller (2008), Resolution of direction of oceanic magnetic lineations by the sixth-generation lithospheric magnetic field model from CHAMP satellite magnetic measurements, *Geochem. Geophys. Geosyst.*, *9*, Q07021, doi:10.1029/2008GC001949.
- Maus, S., C. Manoj, J. Rauberg, I. Michaelis, and H. Lühr (2010), NOAA/NGDC candidate models for the 11th generation International Geomagnetic Reference Field and the concurrent release of the 6th generation Pomme magnetic model, *Earth Planets Space*, *62*, 729–735.

- Reigber, C., H. Lühr, and P. Schwintzer (2003), *First CHAMP Mission Results for Gravity, Magnetic and Atmospheric Studies*, Springer, Berlin, doi:10.1007/978-3-540-38366-6.
- Richmond, A. D., and A. Maute (2014), Ionospheric electrodynamics modeling, in *Modeling the Ionosphere-Thermosphere System*, pp. 57–71, John Wiley, Chichester, U. K., doi:10.1002/9781118704417.ch6.
- Rishbeth, H. (1971), The F-layer dynamo, *Planet. Space Sci.*, *19*, 263–267.
- Rishbeth, H. (1997), The ionospheric E-layer and F-layer dynamos—A tutorial review, *J. Atmos. Sol. Terr. Phys.*, *59*(15), 1873–1880, doi:10.1016/S1364-6826(97)00005-9.
- Stening, R. (1992), Modelling the low latitude F region, *J. Atmos. Terr. Phys.*, *54*(11–12), 1387–1412, doi:10.1016/0021-9169(92)90147-D.
- Thébault, E., et al. (2015), Evaluation of candidate geomagnetic field models for IGRF-12, *Earth Planets Space*, *67*, 112, doi:10.1186/s40623-015-0273-4.